ELECTRONIC SUPPLEMENTARY INFORMATION

Interaction of Triarylmethyl Radical with DNA Termini Revealed by Orientation-Selective W-band Double Electron-Electron Resonance Spectroscopy

Matvey V. Fedin,[1,5,*] Georgiy Yu. Shevelev,[3,5] Dmitrii V. Pyshnyi,[3,5] Victor M. Tormyshev,[4,5] Gunnar Jeschke,[2] Maxim Yulikov,[2,*] Elena G. Bagryanskaya[4,5,*]

[1] International Tomography Center SB RAS, Novosibirsk, 630090, Russia

[2] Laboratory of Physical Chemistry, ETH Zurich, Zurich, 8093, Switzerland

[3] Institute of Chemical Biology and Fundamental Medicine SB RAS, Novosibirsk, 630090, Russia

[4] N. N. Vorozhtsov Novosibirsk Institute of Organic Chemistry SB RAS, Novosibirsk, 630090, Russia

[5] Novosibirsk State University, Novosibirsk, 630090, Russia

I. Calculation of the excited orientations

First, we need to assess the orientation selectivity of the mw pulses. For this sake, we used the obtained parameters of the simulated ED EPR spectra (*g* tensor, linewidths) and experimental settings of pump/probe pulses (see Experimental section of the main text). Note that the excitation bandwidth of the mw pulses was rather small (~0.3 mT for a ~100 ns π-pulse); however, the ED EPR spectrum is strongly broadened due to the *g* strain (distribution of resonance fields). At X band the linewidth of TAM in frozen solution does not exceed ~0.2 mT (FWHM)[S1], whereas at W band the broadening imposed in simulations via *g* strain is equivalent to ~0.65 mT (FWHM, Gaussian). Therefore, the effective excitation bandwidth of mw pulses applied to the TAM radical at W-band is dominated by the distribution of resonance fields (*g* strain). Taking a convolution of two Gaussians (FWHM~0.3 mT from the mw pulse length and ~0.65 mT from *g* strain), we estimate the effective excitation bandwidth of pump/probe pulses as ~0.7 mT resulting in the relatively weak orientation selectivity shown in Figure 2b of the main text. Still it is evident that the probe pulse in pump/probe position 1 excites $g_{\parallel}$ orientations (the poles of the spheres, azimuthal angles near 0 and 180^{o}) more efficiently than $g_{\perp}$ ones (the equators of the spheres, azimuthal angles near 90^{o}). In pump/probe position 2 this trend becomes less obvious, and it completely disappears in pump/probe position 3. These findings are in good agreement with the observed orientation selectivity for dsDNAs **I**-**II**.

S1 A. A. Kuzhelev, D. V. Trukhin, O. A. Krumkacheva, R. K. Strizhakov, O. Y. Rogozhnikova, T. I. Troitskaya, M. V. Fedin, V. M. Tormyshev, E. G. Bagryanskaya, *J. Phys. Chem. B,* 2015, **119**, 13630.

II. Simulations using Model 1

Model 1 assumes that TAM labels are rigidly fixed at dsDNA. Figure S1 complements Figure 1 of the main text and sketches the spin-spin vector AB with respect to the laboratory frame, as well as the molecular frames of the TAMs with respect to the spin-spin vector. The coordinate system (*X*,*Y*,*Z*) is the laboratory frame, where the magnetic field *B* is oriented along *Z*. The coordinate system (*x*,*y*,*z*) is the molecular frame of TAM, and the plane (*x*,*y*) is perpendicular to the C_3 symmetry axis. This plane (*x*,*y*) contains the $g_\perp$ components of the *g* tensor of TAM, whereas the $g_\parallel$ component is directed along the *z* axis of molecular frame, which is the C_3 symmetry axis. θ is the angle between the *z* axis of the molecular frame and the spin-spin vector AB. Since the two terminal base pairs and the two labels are similar, we assume that angle θ is the same for each label. For $\theta \neq 0$, one needs to consider rotation by angle φ around the spin-spin vector AB, which affects orientations of *g* tensors of spins A and B in the laboratory frame. Since we will consider all possible rotations of vector AB around its axis, it is sufficient to fix the inter-radical torsion angle $\Delta\varphi$. Finally, angle ψ accounts for the inclination of vector AB with respect to the laboratory-frame *Z* axis, i.e. with respect to the magnetic field.

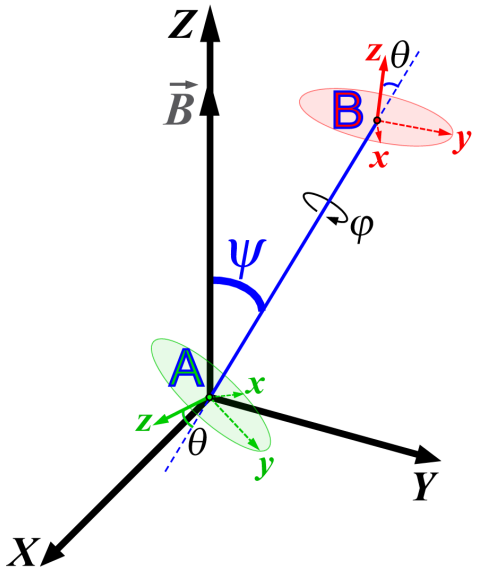

Figure S1. Layout of all coordinate frames used in simulations.

Thus, in the framework of Model 1, we fix two values θ and $\Delta\varphi$. We consider a uniform spherical distribution of orientations of vector AB in the laboratory frame. For each orientation we calculate the probability density (per unit solid angle) of the pump pulse to excite spin B, and simultaneously for the probe pulse to excite spin A (denoted as P_{AB}). For this sake we use

pump/probe distributions calculated using the experimental parameters, which are presented in Figure 4 of the main text. Finally, we obtain the dependence P_{AB} as a function of ψ.

Using this approach, we have calculated a "library" of $P_{AB}(\psi)$ dependences for different values of θ and $\Delta\varphi$. Representative data are shown in Figure 5 of the main text; here we present more data for θ=10, 20, 30, 40, 50, 60, 70, 80, 90° and $\Delta\varphi$=0, 30, 60, 90, 120, 150, 180°. It is evident, that in our experimental conditions the shape of $P_{AB}(\psi)$ does not strongly depend on $\Delta\varphi$. At the same time, its dependence on θ is crucial, as is discussed in the main text.

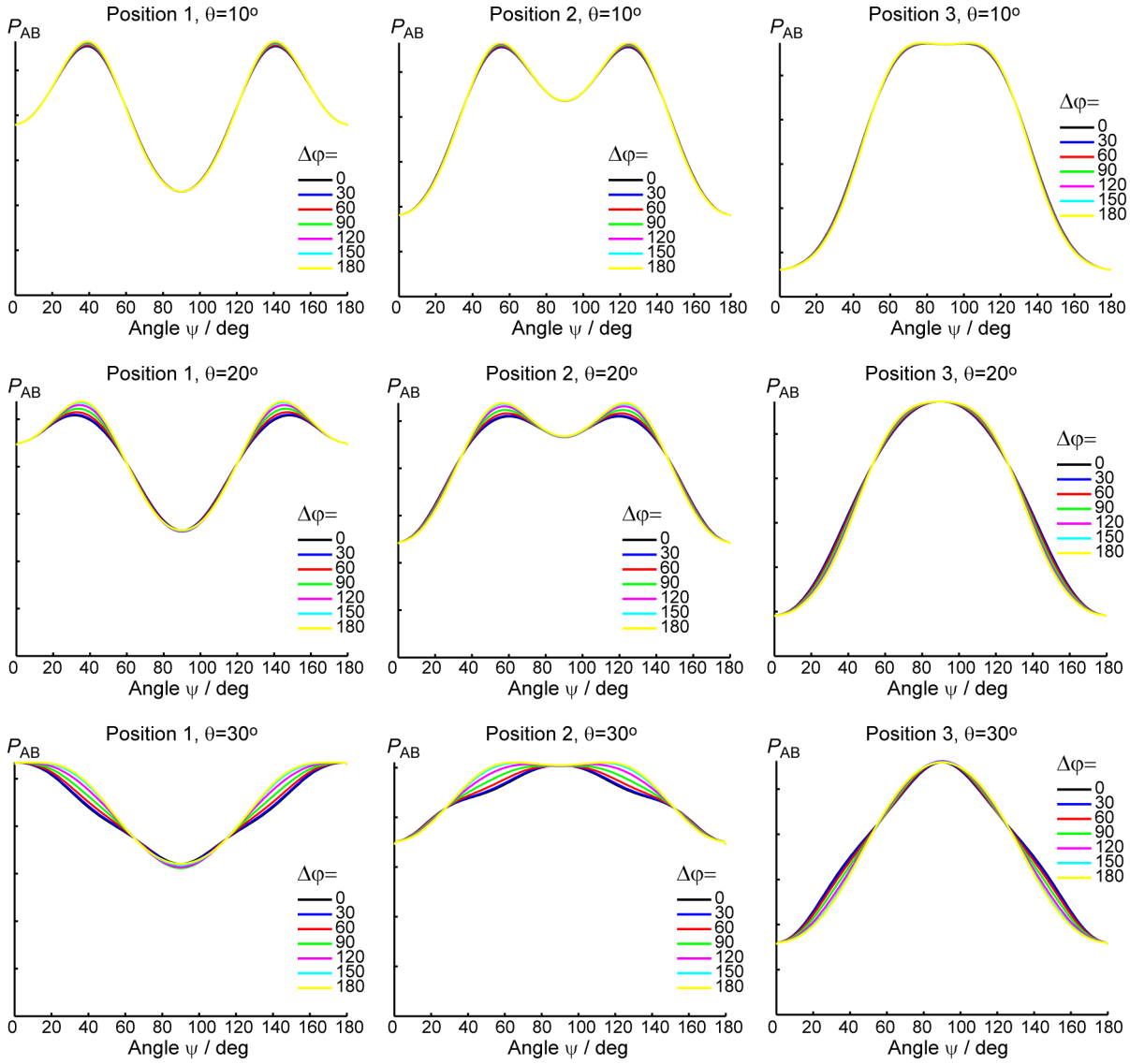

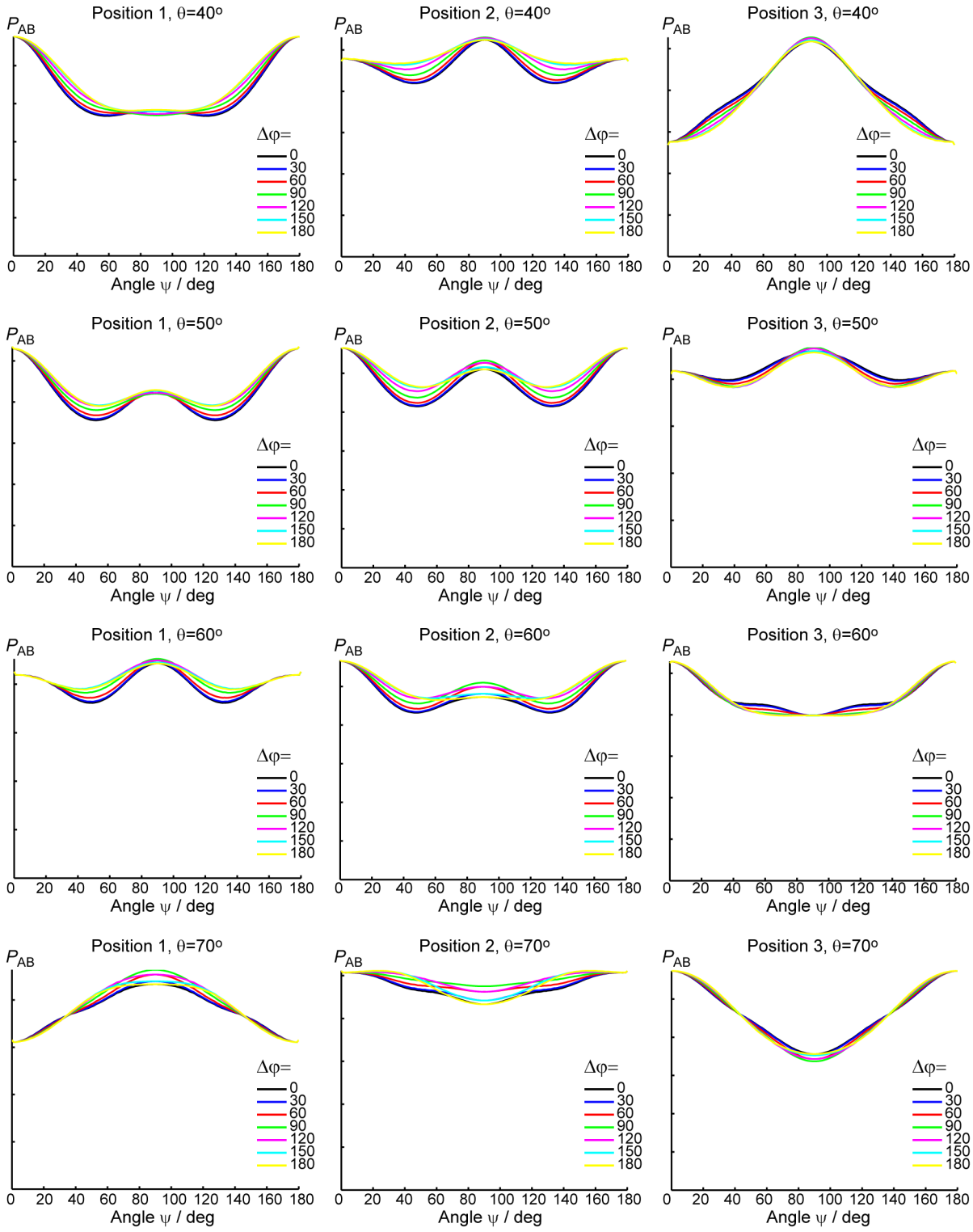
Position 1, θ=40°
Position 2, θ=40°
Position 3, θ=40°
Position 1, θ=50°
Position 2, θ=50°
Position 3, θ=50°
Position 1, θ=60°
Position 2, θ=60°
Position 3, θ=60°
Position 1, θ=70°
Position 2, θ=70°
Position 3, θ=70°
P_AB
Δφ=
0
30
60
90
120
150
180
0 20 40 60 80 100 120 140 160 180
Angle ψ / deg

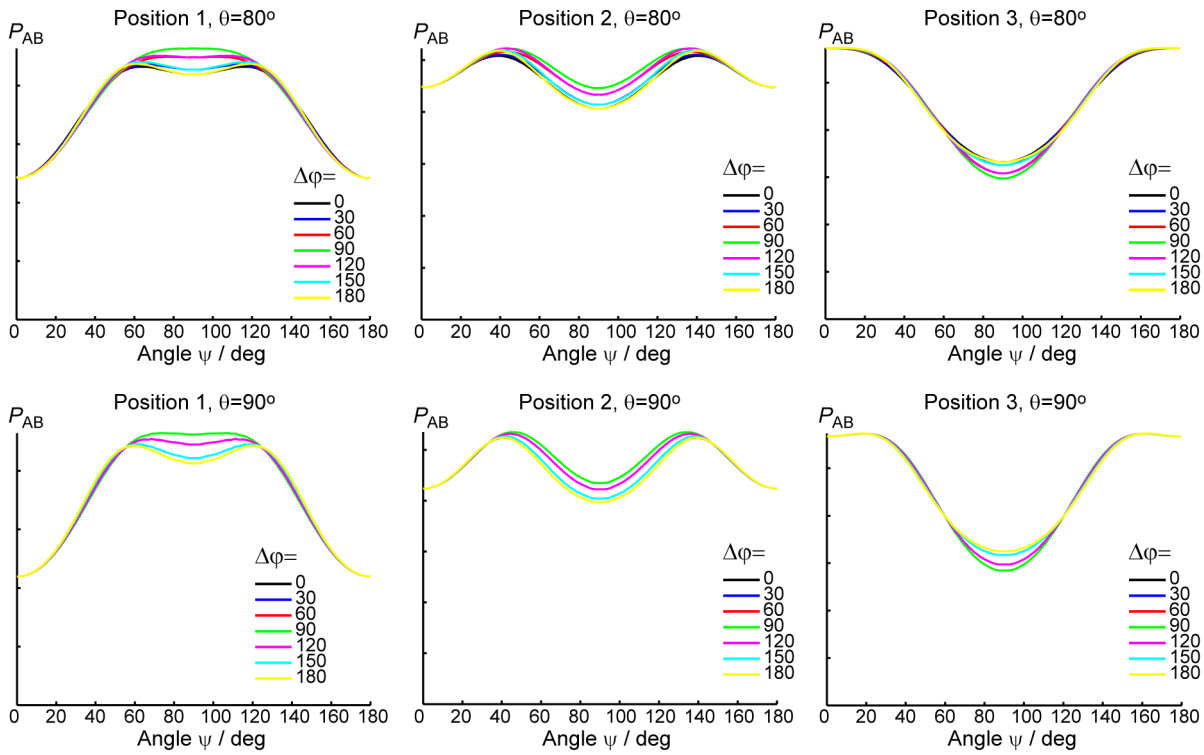

Figure S2. Calculated probability density $P_{AB}(\psi)$ of finding the spin-spin vector AB at an inclination ψ with respect to the magnetic field (Z axis of the laboratory frame). The simulations correspond to Model 1 for dsDNA **II** and to the three pump/probe positions indicated in Figure 2 of the main text. The parameters of the model, angles θ and Δφ, are indicated on the plots. Note that all P_{AB} curves are shown in the interval [0 1] of the ordinate axis.

As follows from Figure S2, qualitative trends observed in experiment are coherent with θ values smaller than roughly 40°. The enhancement of $P_{AB}(\psi)$ at ψ near the poles (0 and 180°) and simultaneous suppression of $P_{AB}(\psi)$ at ψ~90° in pump/probe position 1 is most evident for θ~20-40°; at the same time, the opposite trend is observed in pump/probe positions 2 and 3.

III. Simulations using Model 2

Model 2 uses the same layout of coordinate frames as Model 1 (Fig.S1). However, in Model 2 the orientations of each radical toward vector AB and toward each other are not fixed, but only sterically restrained. We assume that the directions of the molecular-frame z axis of each TAM are randomly distributed inside the cone with opening angle θ_{max} (sketched in Figure S3). In this model, angle φ is not considered due to the axial symmetry of the system, and the only parameter of the model is θ_{max}.

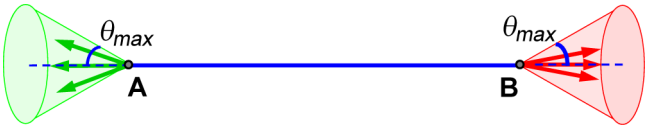

Figure S3. Illustration of specifics of Model 2 (restricting angle θ_{max}).
Red and green arrows show the direction of the molecular frame axis z of TAM.

Again, we consider a uniform spherical distribution of orientations of vector AB. For each orientation we calculate the probability of the pump pulse to excite spin B, and simultaneously for the probe pulse to excite spin A (denoted as P_{AB}). The obtained dependence P_{AB} as a function of ψ is shown for θ_{max}=10, 30, 60 and 90° in Figure S4.

One observes that the results of Model 2 are similar to those of Model 1, in particular when comparing small fixed angles θ in Model 1 and small cone angles θ_{max} in Model 2. The results for θ_{max}=10° closely correspond to the results obtained using Model 1 for θ=10° and various $\Delta\varphi$. For θ_{max}=90° we obtain P_{AB}=const(ψ), because this case effectively covers all arbitrary orientations of TAMs relative to AB. For θ_{max}<30° we obtain $P_{AB}(\psi)$ dependences, which agree reasonably with experimentally observed trends: enhancement of orientations near the poles (ψ~0 and 180°) and suppression of orientations near the equator (ψ~90°) in pump/probe position 1, and the opposite trend in pump/probe positions 2 and 3). However, contrary to Model 1, Model 2 predicts that θ_{max}=60° also allows for the same trends to be observed (although to a lesser extent). This difference of the results obtained using Models 1 and 2 is very reasonable, because Model 2 accounts for all orientations of TAM's z axis inside the cone with opening angle θ_{max}, which includes many orientations with θ close to zero.

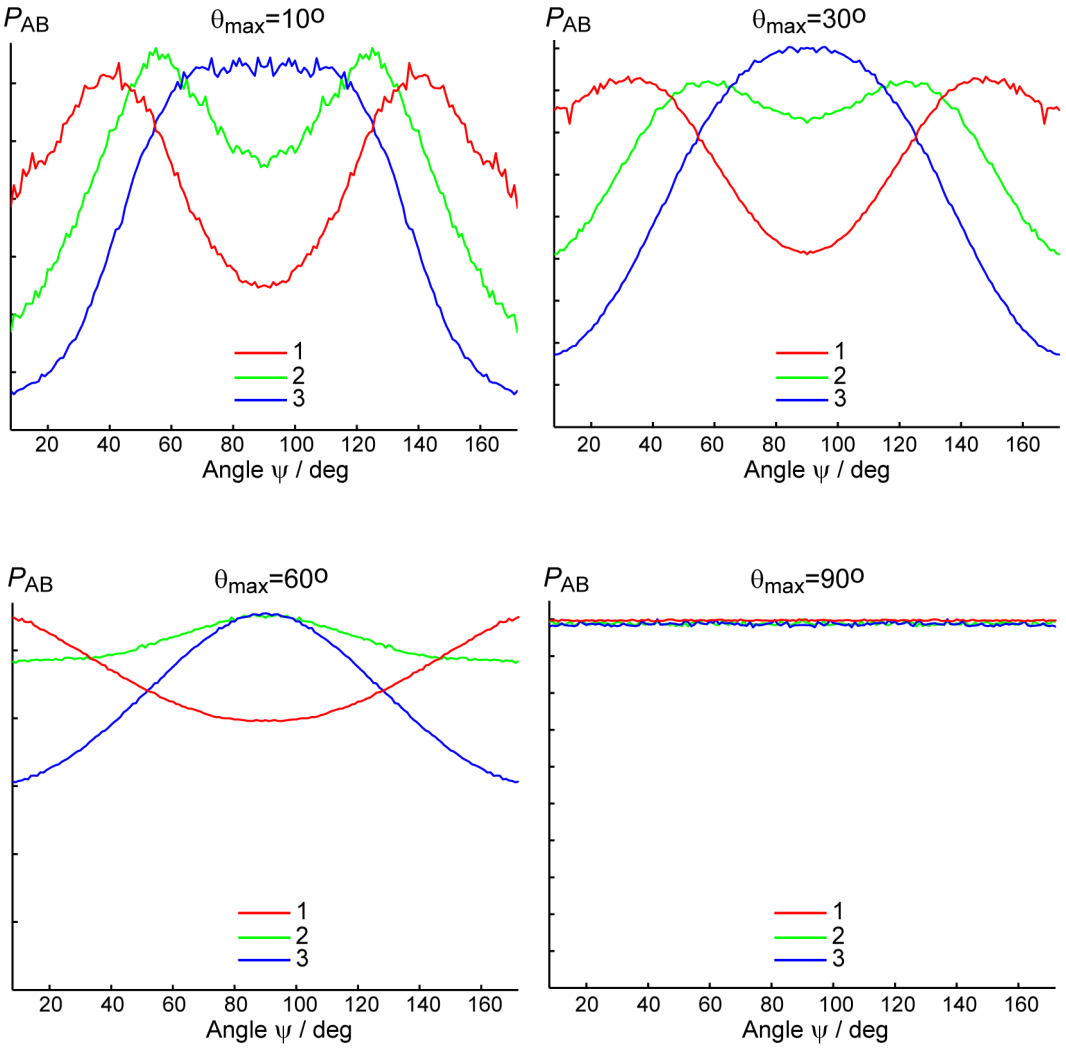

Figure S4. Calculated probability of finding spin-spin vector AB at angle ψ toward the magnetic field (Z axis of laboratory frame). Model 2 for dsDNA **II** and three pump/probe positions indicated in Figure 2 of the main text and shown in the plots of Fig.S4 by numbers. The parameter of the model θ_{max} is indicated on the plots. Note that for visibility all P_{AB} curves are normalized to the density of orientations at each ψ (i.e. uniform distribution would result in P_{AB}=const(ψ)); they are all shown in the interval [0 1] of the ordinate axis.

In conclusion, both theoretical models (Model 1 of fixed labels and Model 2 of sterically restrained labels) necessarily require ordering of the spin labels relative to the dsDNA helix axis to comply with experimentally observed trends. If labels are rigidly fixed (Model 1), θ angle should be rather small (see Fig.S1), roughly θ<30-40°. If labels are randomly distributed with steric restraint θ<θ_{max} (see Fig.S3), a larger range of orientations agrees with experimental data; however, again, approaching θ_{max}=90° leads to the disappearance of any orientation selection.

IV. Original DEER data and processing

Original DEER trace | Form-factor & fit | Frequency-domain spectrum

dsDNA I pump/probe position 1

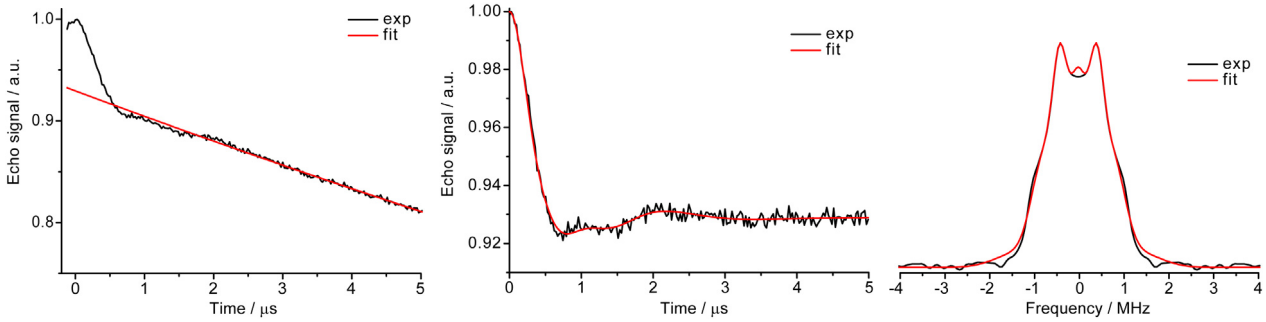

dsDNA I pump/probe position 2

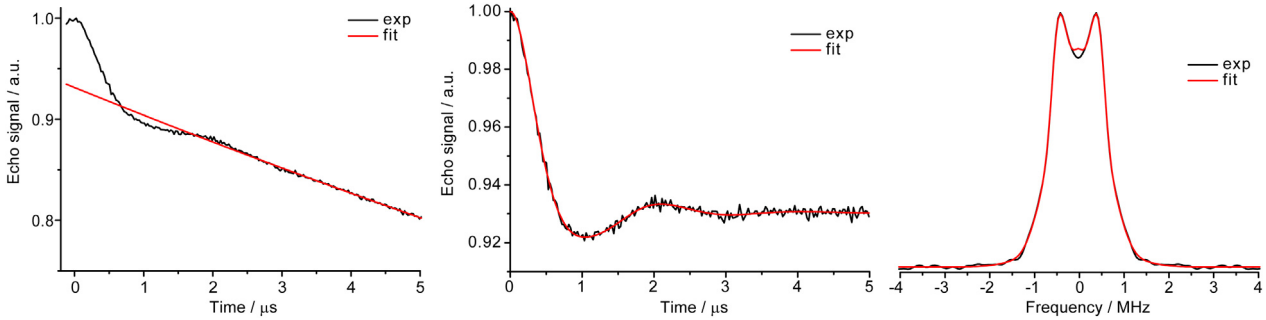

dsDNA I pump/probe position 3

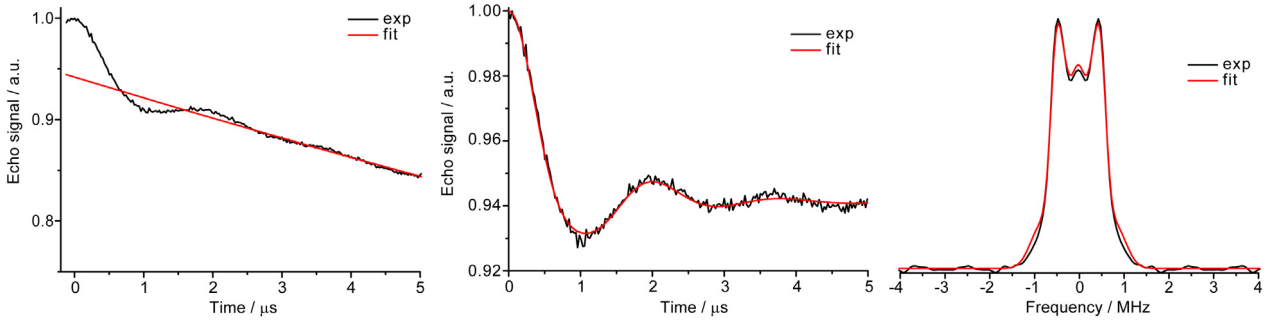

dsDNA II pump/probe position 1

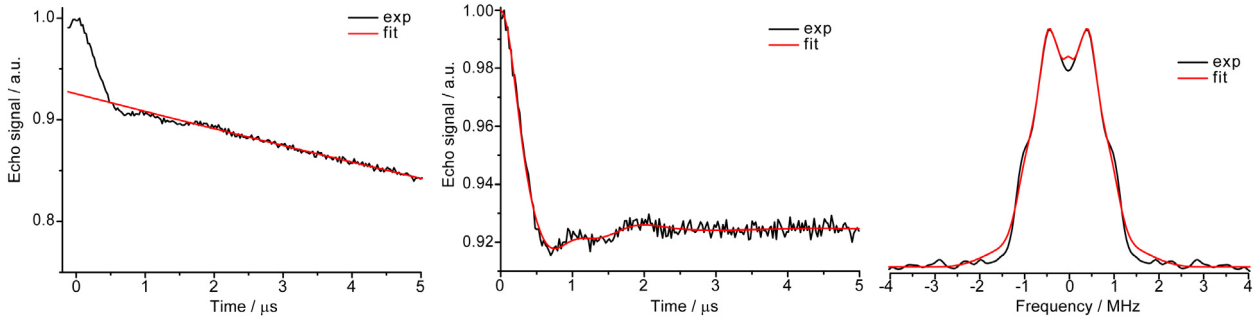

dsDNA II pump/probe position 2

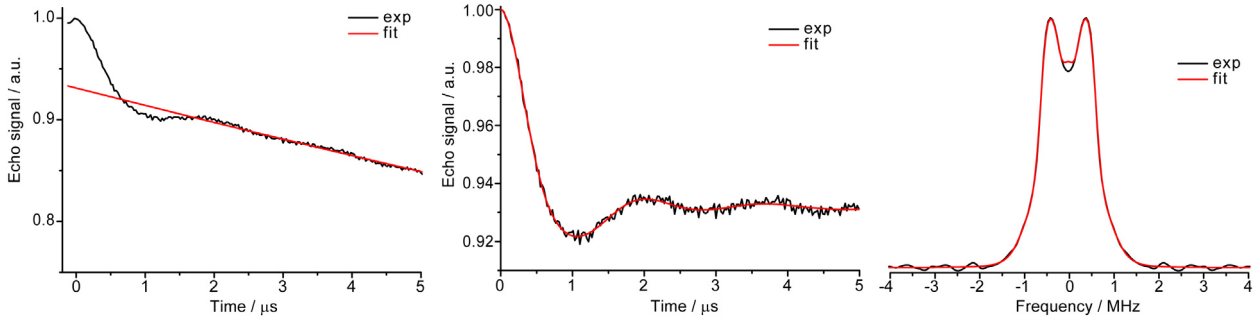

dsDNA II pump/probe position 3

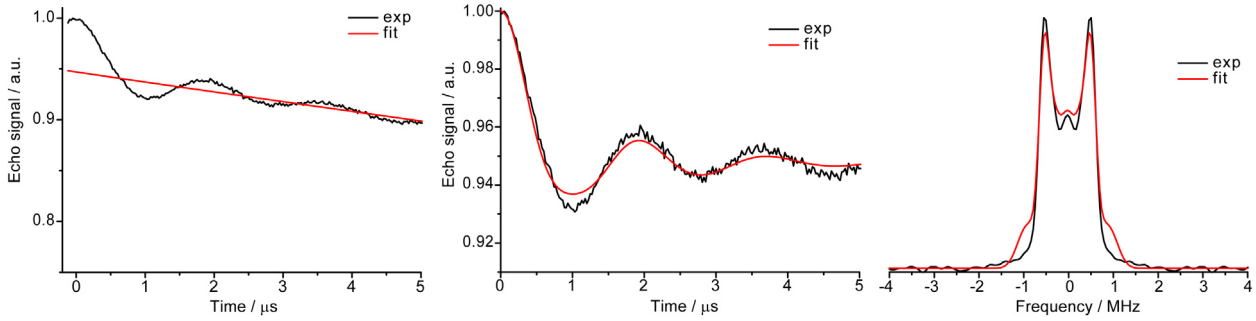

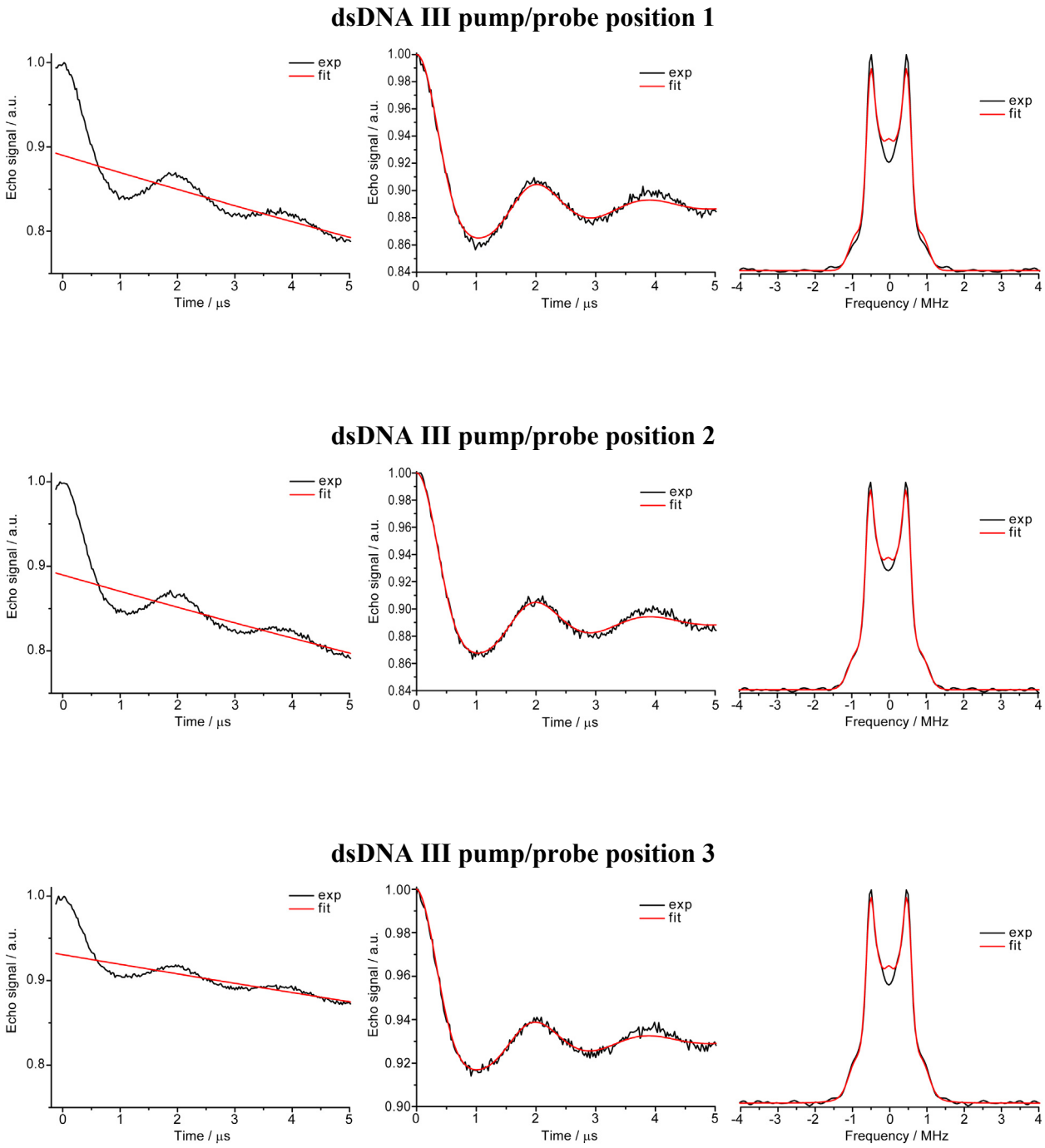

Figure S5. Original DEER data and processing.

Note that in the case of dsDNA **III** the agreement between experimental and simulated frequency-domain spectra is rather good for all 3 pump/probe positions. At the same time, for dsDNAs **I-II** the simulation of frequency-domain spectrum systematically underestimates the parallel component of the Pake pattern in position 1 and overestimates it in position 3, whereas in position 2 the agreement is very good. This trend agrees well with our conclusions on higher orientation selectivity in positions 1 and 3 and weak selectivity in position 2 (see Figure 2b of the main text).

V. Simulation of DEER time-domain data

As was already mentioned in the main text of the paper, our theoretical considerations in this work are auxiliary. The presence of orientation selection unambiguously means there are specific interactions between TAM label and dsDNA termini, but the experimentally achieved orientation selectivity of the mw pulses is only moderate due to the small *g*-anisotropy and large *g*-strain of the TAM labels. Therefore, we aim only at qualitatively reproducing the experimentally observed trends by model calculations. The relevant mismatches between $P_{AB}(\psi)$ values at $\psi \approx 0$ and 90^0 are considered as good qualitative agreement of theoretical modeling with experimental data.

Following this strategy, we have attempted to simulate the time-domain DEER data of dsDNA **II** in pump/probe positions 1-3 using theoretically obtained probability densities shown in Figure 4b of the main text (Figure S6, $\theta = 30^o$ and $\Delta\varphi = 0$). In all cases we used a value of the spin-spin distance of 4.5 nm (dipolar frequency 0.57 MHz) normally distributed with σ=0.15-0.40 nm, i.e. the values well corresponding to those shown in Figure 3b of the main text. The fit is rather good for pump/probe position 3, less good for position 2, and poor for the pump/probe position 1 where the orientation selection is maximum. The calculated probability density leads to the DEER time trace having qualitative indications of the double dipolar frequency, but its contribution is noticeably smaller than in experiment. This means that the calculated $P_{AB}(\psi)$ is overestimated near $\psi \approx 90^0$. For a demonstration purpose, we applied a linear transformation to the calculated $P_{AB}(\psi)$ in pump/probe position 1 in order to enhance the qualitative trend (see inset in Figure S6 top, purple trace "modified"). As a result, the quality of the fitting has drastically improved. Thus, although the calculated $P_{AB}(\psi)$ functions do not allow perfect fitting of DEER time-domain data in all three pump/probe positions, still they provide good qualitative agreement with experimental trends.

The simulation of the dipolar spectra confirms the same trend (Figure S7). The double-frequency shoulder is noticeably enhanced in pump/probe position 1 compared to positions 2 and 3, but this enhancement is still ~2 times weaker than the experimentally observed one. Thus, there is evident qualitative agreement of theory with experiment.

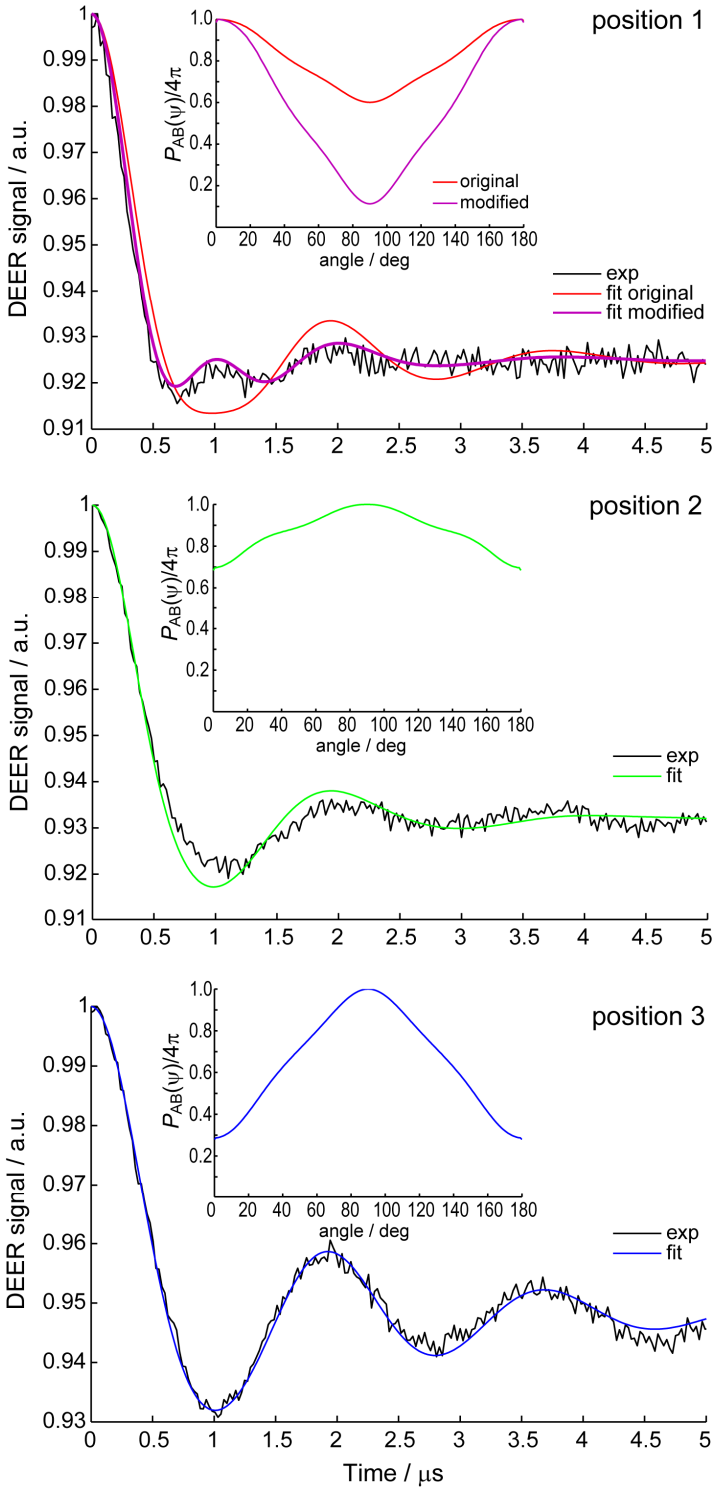

Figure S6. Simulation of DEER time-domain data for dsDNA **II** in pump/probe positions 1-3. Insets reproduce the probability densities shown in Figure 4b of the main text (θ =30° and $\Delta\varphi$=0). In addition, purple trace for position 1 ("modified") shows linear transformation of the original distribution.

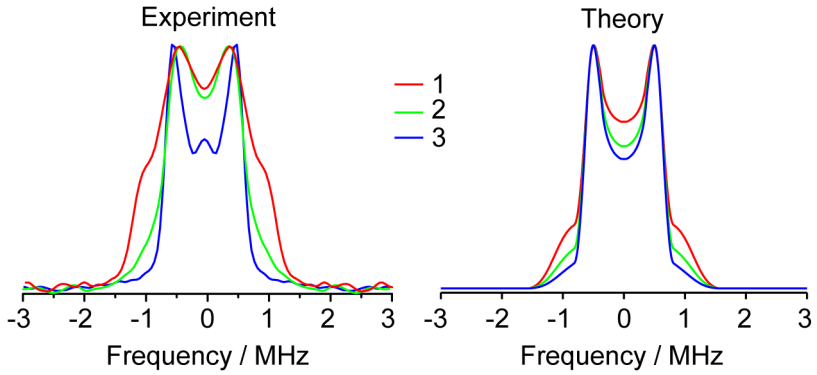

Figure S7. Simulation of DEER frequency-domain data for dsDNA **II** in pump/probe positions 1-3. The experimental data (on the left) is the same as that shown in Figure 3d of the main text. The calculated data (on the right) is obtained using the probability densities shown in Figure 4b of the main text (θ=30^{o} and $\Delta\varphi$=0).

VI. Different conformations of TAM capping the DNA terminal base pair

Figure S8 shows several typical structures of TAM-labeled dsDNA I based on the molecular dynamics calculations presented previously in Ref.S2. All these conformations are the 'capped' ones, where TAM radical approaches closely the terminal base pair; at the same time, calculated spin-spin (TAM-TAM as shown in Figure S8) distances are ≈4.5 nm. The distances between highlighted (red) atoms of TAM and highlighted atoms of DNA are within 0.2 nm, corresponding to the close TAM-DNA contact.

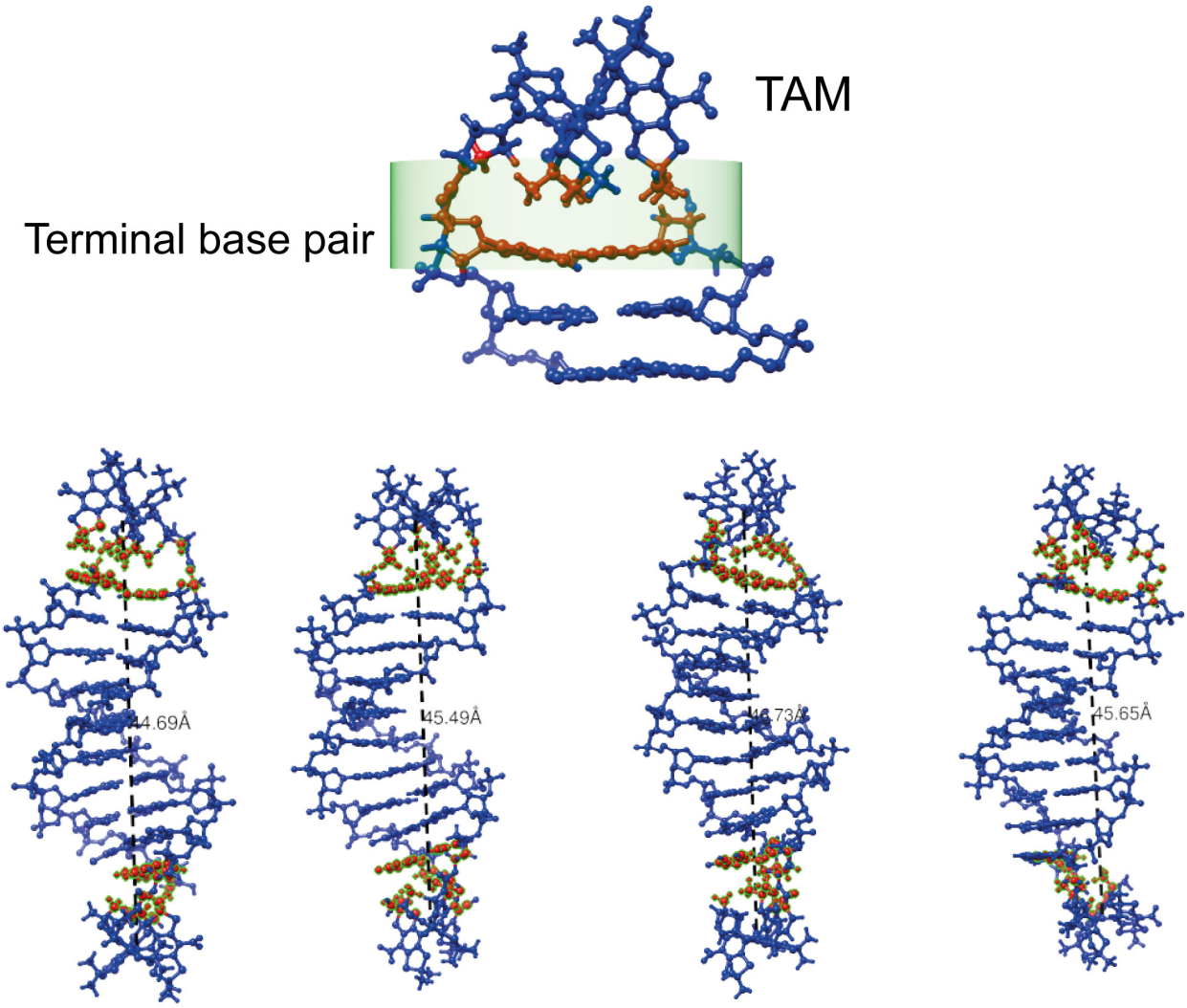

Figure S8. Several different structures of TAM-labeled DNA duplex. Red color of atoms highlights close contacts within 2.0 Å between TAM label and terminal base pair of DNA.

S2 G. Y. Shevelev, O. A. Krumkacheva, A. A. Lomzov, A. A. Kuzhelev, D. V. Trukhin, O. Y. Rogozhnikova, V. M. Tormyshev, D. V. Pyshnyi, M. V. Fedin, E. G. Bagryanskaya, *J. Phys. Chem. B,* 2015, **119**, 13641.